Discovery of an extended halo of stars in the Andromeda spiral galaxy

Puragra Guhathakurta*, James C. Ostheimer†#, Karoline M. Gilbert*, R. Michael Rich‡, Steven R. Majewski†, Jasonjot S. Kalirai*, David B. Reitzel‡, & Richard J. Patterson†

* University of California Observatories/Lick Observatory, University of California at Santa Cruz, 1156 High Street, Santa Cruz, California 95064, USA

† Department of Astronomy, University of Virginia, PO Box 3818, Charlottesville, Virginia 22903, USA

‡ Department of Astronomy, University of California at Los Angeles, Box 951547, Knudsen Hall, Los Angeles, California 90095, USA

Present address: 1810 Kalorama Road NW, #A3, Washington, District of Columbia 20009, USA

Understanding the formation of galaxies and their structural components is a key goal of modern cosmology. Spiral galaxies like our own consist of a planar disk, a bright central bulge whose density decreases exponentially with increasing radius, and an extended halo whose density scales as an inverse power of radius. It is difficult to study our Galaxy's structure from within, but our neighbouring galaxy, the Andromeda spiral (M31), offers a global external perspective and yet is close enough for us to resolve individual stars. Studies of M31^{1–3} have concluded that its outer spheroid is an extension of its inner bulge, displaying the characteristic exponential decline out to a radius of 20 kiloparsecs^{4,5}. We report here on the discovery of a smooth *halo* of M31 red giant stars extending beyond r = 150 kiloparsecs with an r^{-2} projected profile like M31's globular cluster population⁶. The density of these stars is well above the outward extrapolation of the bulge

brightness profile. Characterizing the dynamics, metallicity, substructure, and age of this M31 halo will provide unique tests of galaxy formation theories^{7–9}.

Galaxies come in a rich variety of shapes and sizes. Ellipticals anchor one end of the "Hubble morphological sequence" of galaxies while dwarf irregulars lie at the other end¹⁰. Spirals lie between these two galaxy types in the sequence and each contain three subcomponents: disk, bulge, and halo. Bulges and halos are both spheroidal in shape but bulges have a higher central density, a sharper density decline in their outskirts (exponential vs. power-law), and a higher abundance of heavy elements ("metallicity"). Disks form stars at a steady rate over their lifetime; by contrast halo stars [at least in the Milky Way (MW)] formed early in its history and/or were acquired via the accretion of satellite galaxies. The formation and evolution of these galactic subcomponents continues to be the subject of intense theoretical and observational research^{7,9,11,12}.

The MW and its nearest large neighbour the Andromeda galaxy (M31) contain clues about the events that shaped their formation just as a fossil bears a historical record. For example, debris trails seen in the two galaxies 13,14 provide direct evidence of ongoing accretion of small satellites as predicted by hierarchical structure formation models $^{7-9}$. The differences between the two galaxies may result from the stochastic nature of these processes: M31's bulge is larger and more luminous than the MW's, and its outer spheroid ($r \sim 10-30 \text{ kpc}$) has a steeper radial brightness profile and is denser and $r = 10 \times 10^{16}$ more metal-rich bear a steeper radial brightness profile that is denser for the presence of obvious substructure $r = 10 \times 10^{16}$ more metal-rich spheroid surface brightness follows a "de Vaucouleurs $r = 10 \times 10^{16}$ (characteristic of bulges) from the centre out to 20 kpc on the minor axis. Does this galaxy have only a single (field star) spheroidal component, a bulge, in contrast to the bulge and halo seen

_

^a The distance to M31 is assumed to be 783 kpc throughout this letter.

^b Surface brightness as a function of radius is given by: $\Sigma(r) = \Sigma_0 \exp[-7.67(r/r_e)^{1/4}]$.

in other spirals? M31 is known to contain a population of halo globular clusters with an r^{-2} surface density distribution⁶, but is there no associated halo field star population?

In this letter we present evidence for a halo of red giant branch (RGB) stars in M31 with a $\Sigma(r) \propto r^{-2}$ surface density profile. The population extends out to a projected radius >150 kpc, as measured along the south-east minor axis, implying that the galaxy is much larger than previously thought. We show that the crossover between halo and bulge occurs at a minor-axis distance of ≈ 30 kpc, showing that most previous studies of the "M31 spheroid" have been sampling the outer parts of its bulge rather than its halo.

The proximity of M31 makes it easy to *detect* its brightest RGB stars but it is difficult to *isolate* sparse groups of such stars from the dense screen of foreground MW dwarf star and background galaxy contaminants. We combine three methods to identify these rare RGB stars: (**A**) wide-field imaging/photometry through the *DDO*51 filter¹⁷; (**B**) medium resolution Keck spectroscopy of RGB candidates^{20–22}; and (**C**) a new probabilistic method for separating M31 RGB from MW dwarf stars using spectral and photometric diagnostics²³. Method **A** discriminates between these two types of stars to a large degree: the intermediate width ($\Delta\lambda \approx 12$ nm) *DDO*51 band includes the 517 nm MgH/Mgb stellar absorption feature that is weak (strong) in low (high) surface gravity RGB (dwarf) stars^{17–19}. Method **B** yields the radial velocity, based largely on the crucial 850 nm CaII absorption line triplet that is prominent in cool stars, and stellar absorption line strengths; these, plus the *DDO*51 parameter, serve as input data for method **C**.

The imaging survey¹⁷ in the DDO51 band and Washington system M and T_2 bands was carried out with the Mayall 4-m telescope at Kitt Peak National Observatory (KPNO) and Mosaic camera during 1998–2001. Each Mosaic field covers $36' \times 36'$.

Nine such fields are shown in Figure 1 spanning the radial range $2^{\circ}-12^{\circ}$ to the south of M31. Exposure times are $\approx 0.25-1.5$ hr per filter per field. Standard data reduction techniques are used to obtain photometry for each object and to determine if it is broader than the $\approx 1''$ seeing point spread function. The photometry is corrected for reddening by foreground dust²⁴ and transformed to the Johnson/Cousins (V, I) system. Each object is assigned a DDO51 parameter (≈ 1 and 0 for RGB and dwarf stars, respectively) based on its location relative to the narrow locus of dwarf stars in the (M–DDO51) vs. (M– T_2) colour-colour diagram¹⁹. M31 RGB candidates^c are defined as objects having a DDO51 parameter > 0.5 and star-like image morphology.

Figure 2 shows the surface brightness profile derived from counts of RGB candidates in our sample (squares). The conversion to *V*-band surface brightness units is done using a globular cluster luminosity function¹⁷. A constant "background" (dashed line) is subtracted to statistically remove sample contaminants: compact field galaxies and foreground MW dwarf stars. The background level is optimized using the spectroscopic sample (see below); the associated uncertainty is about 15%¹⁸.

The two data points based on our RGB candidates at $r \approx 20$ kpc (squares in Fig. 2) agree with previous measurements⁴ (crosses); these data lie well above the background (dashed line) and this makes them immune to background uncertainties. The surface density of RGB stars relative to contaminants at r > 50 kpc is so low that DDO51-based selection is not efficient enough for us to reliably measure M31's surface brightness.

Spectroscopy of M31 RGB candidates²⁰ in 5 fields (blue squares in Fig. 1) was carried out with the Keck II 10-m telescope and DEIMOS in 2002–2003. Data from 11

_

^c The term "RGB candidates" is used to refer to stars that satisfy these *DDO*51 and morphology criteria, while "RGB stars" refers to spectroscopically confirmed objects.

multi-slit masks are analyzed here, each with 75–100 slits on RGB candidates and lower priority "filler" targets in the brightness range $20 < I_0 < 22.5$. The slit width is 1". The seeing FWHM is 0.8"–1.0". The 1200 line mm⁻¹ grating covers the wavelength range 640–910 nm at a resolution of 0.15 nm. The exposure time is 1.0–1.5 hr per mask. The data are processed using the SPEC2D software to obtain sky-subtracted two- and one-dimensional spectra; the 1D spectra are cross-correlated against spectral templates to obtain radial velocity estimates using SPEC1D; the results are verified using ZSPEC^d.

Background galaxies are easily removed from the sample on the basis of redshift. Telling M31 RGB from MW dwarf stars is more difficult. A new probabilistic method based on 5 diagnostics is used to separate these two stellar types^{20,23}: (1) radial velocity, (2) *DDO*51 parameter, (3) strength of the surface-gravity-sensitive NaI absorption line doublet at 819 nm vs. (*V–I*)₀ colour, (4) location in the colour-magnitude diagram (CMD), and (5) comparison of the *spectroscopic* metallicity, inferred from the strength of the CaII absorption line triplet at 850–866 nm, with the *photometric* metallicity, inferred from the CMD location relative to theoretical RGB tracks. Samples drawn from fields close to (far from) M31's centre yield a "training set" of definite RGB (dwarf) stars. Analytical fits to the distribution of training set stars are used as empirical RGB and dwarf star probability distribution functions (PDFs) for each diagnostic.

Figure 3(a–d) illustrates diagnostics 1, 2, 3, and 5, respectively. The NaI doublet is stronger in cool dwarfs than in cool RGB stars; the CaII-based metallicity estimate agrees with the photometric estimate for RGB stars but is weaker for dwarf stars. The RGB and dwarf PDFs have significant overlap in all cases: no one diagnostic is a

_

^d These software pipelines/tools were developed at UC Berkeley for the DEEP2 project. For details see — http://astron.berkeley.edu/~cooper/deep/spec2d/primer.html.

perfect discriminant. For each star, its properties and the corresponding PDFs are used to compute the probability of its being an RGB and dwarf star, P^i_{giant} and P^i_{dwarf} , for the i^{th} diagnostic. The overall likelihood is defined to be: $L = \sum \log(P_{giant}/P_{dwarf})^i$, where the sum runs over the five diagnostics. The stars in each field have a bimodal distribution of likelihood values with a minimum at $L \approx 0$: those with higher (lower) L values are confirmed M31 RGB (MW dwarf) stars. Figure 3 demonstrates that confirmed RGB stars in fields **m6** and **m11** (bold histograms/symbols) differ from MW dwarf stars (dot-dashed histograms/crosses) in the sense that they follow the RGB PDFs, and not the dwarf PDFs, in terms of *all* of their properties. Moreover, tests using the dwarf star training set show that: (a) the group with L > 0 is *not* merely the tail of the dwarf distribution but rather a distinct population, and (b) the probabilities derived from the different diagnostics are largely independent of one another so their product is an effective RGB/dwarf star discriminant²³.

Keck multi-slit spectroscopic data are also presented for 6 new DEIMOS masks in the inner fields **H11**, **H13s**, and **H13d**, along with previously published LRIS data in the fields **RG02**²¹ and **G1**²² (Fig. 1 inset). *DDO*51 photometry is not available for these 5 inner fields (the high surface density of M31 RGB stars means that the contamination is not too severe here); we instead rely on broadband photometry from a few different sources. Targets are selected from the range $20 < I_0 < 22.5$ as before. For the DEIMOS targets, the RGB/dwarf star likelihood value is based on the four non-*DDO*51 diagnostics. We resort to less reliable statistical RGB-dwarf separation methods for the LRIS fields^{21,22}.

Spectroscopy yields uncontaminated samples of M31 RGB stars, but it is difficult to determine the net yield (success rate) for measuring radial velocities. Fortunately, tests show that this quantity is comparable for M31 RGB and MW dwarf stars in a given mask/field. Thus the *ratio* of RGB to dwarf stars, times the expected surface

density of dwarfs in each field (a function of its Galactic coordinates²⁵), provides a measure of M31's surface brightness. The filled (open) circles in Figure 2 represent the spectroscopic subset with (without) DDO51 pre-selection. Since we want to measure M31's smooth spheroidal component, colder components such as M31 disk RGB stars (in fields **H13d** and **G1**) and members of the giant southern stream (in fields **H13s** and **a3**) are statistically subtracted from the raw RGB counts based on fits to the observed radial velocity distribution 20,22 ; this subtraction introduces additional uncertainty over and above the Poisson errors shown in Figure 3. The two sets of surface brightness measurements (filled and open circles) have been independently normalized to match other measurements at comparable radii (squares, crosses). The empirical relative normalization between the two spectroscopic subsets is 5.0, comparable to the net efficiency boost expected from DDO51 selection 19 . For reasons discussed below, the effective minor-axis distance for the off-axis inner fields **H13d** and **H13s** has been computed using the flattening of b/a = 0.6 measured for M31's inner spheroid^{2,4}.

In contrast to the existing data⁴ that are well fit by a de Vaucouleurs $r^{1/4}$ law plus exponential disk out to $r \approx 20 \text{ kpc}^e$ (crosses in Fig. 2), our new brightness estimates lie well above the extrapolation of the fit for r > 50 kpc (filled circles and squares). This excess is widespread and independent of measurement technique — it applies to photometric samples in fields **m4**, **a19**, **b15**, and **m8** and to spectroscopic and photometric samples fields **a13**, **m6**, and **m11** — and is not just an anomaly in a single field. In fact, our new measurements follow a power-law surface brightness profile, $\Sigma(r) = \Sigma_0 r^{-2.3\pm0.3}$, over the range r = 30-150 kpc (solid line), similar to the slope of the radial distribution of M31 and MW globular clusters⁶. It seems reasonable to label the

-

^e A careful inspection of Figure 2 reveals that the bulge surface brightness falls slightly below the $r^{1/4}$ law fit in the range $r \approx 10-20$ kpc, as was noted over a decade ago⁴.

 $r^{1/4}$ law and r^{-2} power-law components M31's "bulge" and "halo", respectively. M31's halo is estimated to contain less than about 5% of its total luminosity, assuming its density profile flattens off in the inner few kpc.

The unprecedented surface brightness level to which we have traced M31's halo, $\mu_V \approx 35 \text{ mag arcsec}^{-2}$, is well beyond the reach of even the deepest integrated light measurements²⁶ and is a direct result of the effectiveness of our RGB/dwarf separation technique. The M31 halo is assumed to consist of field stars in a smooth spherical configuration; however, the presence of sub-structure (e.g., a superposition of debris trails^{8,9}) and/or an appreciable degree of flattening cannot be ruled out given the limited spatial coverage of our survey. The observed radial velocity distribution of RGB stars in the outer halo fields is consistent with a Gaussian of width $\sigma_{\text{vel}} = 80 \text{ km s}^{-1}$ centred on M31's systemic velocity. The velocity and metallicity distribution of these stars is also consistent with that of the present-day dwarf satellites of M31²⁷.

Could the RGB stars in our outermost fields have come from M31's companion M33? The spectroscopic fields **m11** and **m6** are at projected radii of 50 and 100 kpc from M33, respectively. Even though the mean velocity of the RGB stars in these fields is offset by -120 km s^{-1} with respect to M33's systemic velocity [Fig. 3(a)], that galaxy's internal motions and Poisson errors in our sample are large enough to account for the offset. We cannot rule out the possibility that these RGB stars are part of a broad tidal bridge between M31 and M33²⁸. However, given that M33 is much smaller and less luminous than M31, it is more likely that even the three RGB stars in field **m11** are M31 members with $r_{M31} = 150 \text{ kpc}$ than M33 members with $r_{M33} = 50 \text{ kpc}$.

The large size of M31's halo, r = 150 kpc, and the observed line-of-sight velocity dispersion implies a circular orbital period of nearly 7 Gyr. The period is much shorter (by an order of magnitude or more) for highly eccentric orbits. M31's halo dynamics

will be better characterized as larger spectroscopic samples become available in the near future. It will also be instructive to compare the metallicity distributions of the bulge and halo. Detailed chemical abundance studies may be possible using absorption line strengths in high signal to noise co-added RGB spectra²². Direct age measurements via the main sequence turnoff show that a third of M31's bulge stars are younger than 10 Gyr²⁹. One hopes that such studies can be extended to its newly discovered halo.

Received on 2005 February XX; accepted on 2005 XXX XX.

- 1. de Vaucouleurs, G. Photoelectric photometry of the Andromeda nebula in the UBV system. *Astrophys. J.* **128**, 465–488 (1958).
- Walterbos, R. A. M. & Kennicutt, R. C., Jr. Multi-color photographic surface photometry of the Andromeda galaxy. *Astron. Astrophys. Suppl.* 69, 311–332 (1987).
- 3. Pritchet, C. J. & van den Bergh, S. Observations of RR Lyrae stars in the halo of M31. *Astrophys. J.* **316,** 517–529 (1987).
- 4. Pritchet, C. J. & van den Bergh, S. Faint surface photometry of the halo of M31. *Astron. J.* **107**, 1730–1736 (1994).
- 5. Durrell, P. R., Harris, W. E. & Pritchet, C. J. Photometry and the metallicity distribution of the outer halo of M31. II. The 30 kiloparsec field. *Astron. J.* **128**, 260–270 (2004).
- 6. Racine, R. Globular clusters in the halo of M31. Astron. J. 101, 865–872 (1991).
- 7. Searle, L. & Zinn, R. Compositions of halo clusters and the formation of the galactic halo. *Astrophys. J.* **225**, 357–379 (1978).
- 8. Johnston, K. V., Hernquist, L. & Bolte, M. Fossil signatures of ancient accretion events in the halo. *Astrophys. J.* **465**, 278–287 (1996).

- 9. Bullock, J. S., Kravtsov, A. V. & Weinberg, D. H. Hierarchical galaxy formation and substructure in the Galaxy's stellar halo. *Astrophys. J.* **548**, 33–46 (2001).
- 10. Hubble, E. The realm of the nebulae. New Haven: Yale Univ. Press (1936).
- 11. Eggen, O. J., Lynden-Bell, D. & Sandage, A. R. Evidence from the motions of old stars that the Galaxy collapsed. *Astrophys. J.* **136,** 748–766 (1962).
- 12. Governato, F. *et al.* The formation of a realistic disk galaxy in Λ-dominated cosmologies. *Astrophys. J.* **607**, 688–696 (2004).
- 13. Majewski, S. R., Skrutskie, M. F., Weinberg, M. D. & Ostheimer, J. C. A Two Micron All Sky Survey view of the Sagittarius dwarf galaxy. I. Morphology of the Sagittarius core and tidal arms. *Astrophys. J.* **599**, 1082–1115 (2003).
- 14. Ferguson, A. M. N., Irwin, M. J., Ibata, R., Lewis, G. F. & Tanvir, N. R. Evidence for stellar substructure in the halo and outer disk of M31. *Astron. J.* **124**, 1452–1463 (2002).
- 15. Reitzel, D. B., Guhathakurta, P. & Gould, A. Isolating red giant stars in M31's elusive outer spheroid. *Astron. J.* **116,** 707–722 (1998).
- 16. Rich, R. M., Mighell, K. J., Freedman, W. L. & Neill, J. D. Local Group populations with the Hubble Space Telescope. I. The M31 globular cluster G1=Mayall II. *Astron. J.* **111**, 768–776 (1996).
- 17. Ostheimer, J. C. Exploring the halo of M31. *Ph. D. dissertation*, University of Virginia (2002).
- 18. Ostheimer, J. C. *et al.* M31's extended stellar halo. II. Star-count profile from a DDO51 photometric sample. *Astron. J.* in preparation (2005).
- 19. Majewski, S. R., Ostheimer, J. C., Kunkel, W. E. & Patterson, R. J. Exploring halo substructure with giant stars. I. Survey description and calibration of the photometric search technique. *Astron. J.* **120**, 2550–2568 (2000).

- Guhathakurta, P. et al. Dynamics and stellar content of the giant southern stream in M31. I. Keck spectroscopy of red giant stars. Astron. J. submitted (2005; astro-ph/0406145).
- 21. Reitzel, D. B. & Guhathakurta, P. Metallicity and kinematics of M31's outer stellar halo from a Keck spectroscopic survey. *Astron. J.* **124**, 234–265 (2002).
- 22. Reitzel, D. B., Guhathakurta, P. & Rich, R. M. Keck spectroscopy of red giant stars in the vicinity of M31's massive globular cluster G1. *Astron. J.* **127**, 2133–2138 (2004).
- 23. Gilbert, K. M. *et al.* M31's extended stellar halo. III. A new method for isolating and characterizing a clean sample of red giants. *Astron. J.* in preparation (2005).
- 24. Schlegel, D. J., Finkbeiner, D. P. & Davis, M. Maps of dust infrared emission for use in estimation of reddening and Cosmic Microwave Background Radiation foregrounds. *Astrophys. J.* **500**, 525–553 (1998).
- 25. Ratnatunga, K. U. & Bahcall, J. N. Estimated number of field stars toward Galactic globular clusters and Local Group galaxies. *Astrophys. J. Suppl.* **59**, 63–76 (1985).
- 26. Fry, A. M., Morrison, H. L, Harding, P. & Boroson, T. A. Deep CCD surface photometry of the edge-on spiral NGC 4244. *Astron. J.* **118**, 1209–1219 (1999).
- 27. Evans, N. W., Wilkinson, M. I., Guhathakurta, P., Grebel, E. K. & Vogt S. S. Dynamical mass estimates for the halo of M31 from Keck spectroscopy.
 Astrophys. J. (Letters), 540, L9–L12 (2000).
- 28. Braun, R. & de Thilker, D. A. The WSRT wide-field H I survey. II. Local Group features. *Astron. Astrophys.* **417**, 421–435 (2004).
- 29. Brown, T. *et al*. Evidence of a significant intermediate-age population in the M31 halo from main-sequence photometry. *Astrophys. J.* **592,** L17–L20 (2003).

30. Choi, P. I., Guhathakurta, P. & Johnston, K. V. Tidal interaction of M32 and NGC 205 with M31: Surface photometry and numerical simulations. *Astron. J.* **124,** 310–331 (2002).

The *DDO*51 imaging data were obtained at KPNO of NOAO, which is operated by the AURA, Inc., under cooperative agreement with the NSF. The spectroscopic data were obtained at the W. M. Keck Observatory, which is operated as a scientific partnership among the California Institute of Technology, the University of California and NASA. The Observatory was made possible by the generous financial support of the W. M. Keck Foundation. We are grateful to Chris Pritchet, Marla Geha, and the DEEP2 Redshift Survey and DEIMOS instrument teams, especially Michael Cooper, Sandy Faber, Drew Phillips, Alison Coil, Greg Wirth, Kai Noeske, Jeff Lewis, and Matt Radovan. This project was supported by NSF grant AST-0307966 and NASA/STScI grant GO-10265.02 (P.G., K.M.G., and J.S.K.), an NSF Graduate Fellowship (K.M.G.), NSF grants AST-0307842 and AST-0307851, NASA/JPL contract 1228235, the David and Lucile Packard Foundation, and The F. H. Levinson Fund of the Peninsula Community Foundation (S.R.M., J.C.O., and R.J.P.), and NSF grant AST-0307931 (R.M.R. and D.B.R.).

Correspondence and requests for materials should be addressed to P.G. (e-mail: raja@ucolick.org).

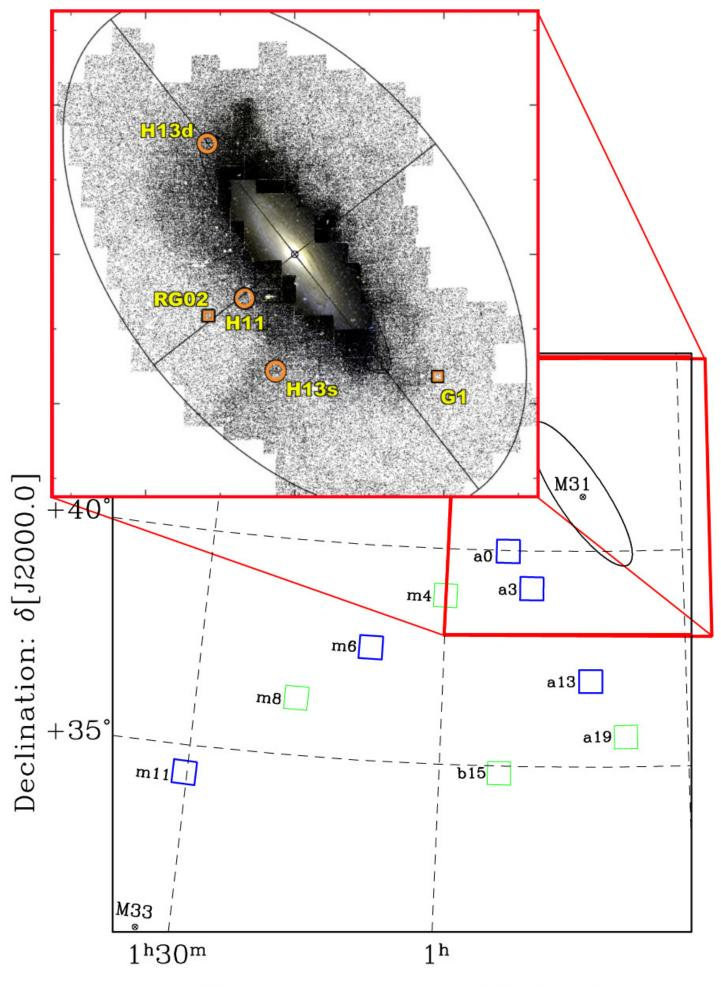
Figure 1 Location of our fields around M31. Blue (green) squares show areas to the south of M31's visible disk (represented by the ellipse) imaged with the KPNO 4-m telescope in the DDO51 band¹⁷, with (without) follow-up spectroscopy using DEIMOS on the Keck 10-m telescope. The $6.5^{\circ} \times 6.5^{\circ}$ bold red square centred on M31 corresponds to the boundary of the inset star-count map¹⁴. The orange circles and squares in the inset indicate areas with Keck spectroscopy using DEIMOS and LRIS, respectively, but with no DDO51 photometry. The CCD mosaic image at the centre of the star-count map shows the visible disk of M31³⁰.

Figure 2 Surface brightness versus (effective) radial distance along M31's minor axis. Previous integrated brightness and star count-based

measurements⁴ (crosses) are well fit by the sum of a de Vaucouleurs $r^{1/4}$ law bulge and an exponential disk (thin solid line) out to 10 kpc. The squares are based on DDO51-selected star counts in our photometric sample¹⁷ (error bars are quadrature sum of Poisson and 15% background subtraction errors), and the dashed line shows the adopted background level¹⁸. The filled (open) circles with Poisson error bars are derived from RGB/dwarf star count ratios in our spectroscopic samples with (without) DDO51 photometric pre-selection. The spectroscopic field names, in order of increasing radius, are: H11, H13d, H13s, RG02, a0, a3, G1, a13, m6, and m11. The RGB count has been statistically corrected for contamination by M31's disk (fields H13d and G1) and giant southern stream (fields H13s and a3) on the basis of radial velocity data. The two sets of spectroscopy-based measurements have been normalized to the other measurements. For the few spectroscopic fields that are off M31's minor axis (Fig. 1), the effective radial distance along the minor axis is calculated assuming a flattening of b/a = 0.6 for r < 30 kpc (bulge) and b/a = 1 for r > 30kpc (halo). Our surface brightness measurements are significantly in excess of the extrapolation of the de Vaucouleurs $r^{1/4}$ law fit to the inner bulge beyond $r \approx$ 50 kpc; in fact, our data are consistent with an $r^{-2.3}$ power law over the radial range 30-150 kpc (bold solid line).

Figure 3 Properties of confirmed M31 red giants in our two outermost spectroscopic fields. Four of the five diagnostics used to distinguish RGB stars from foreground Galactic dwarf star contaminants are illustrated²³. (a) Radial velocity distribution of M31 RGB stars in field **m11** (**m6**) and dwarf stars [shaded (unshaded) bold and dot-dashed histograms, respectively], compared to empirical probability distribution functions derived from training sets consisting of definite RGB and dwarf stars (solid and dashed curves, respectively). The arrow marks the systemic velocity of M31's companion

galaxy M33. (**b**) Same as (**a**) for the *DDO*51 parameter, which is based on the star's location in (M–DDO51) vs. (M– T_2) colour-colour space. (**c**) Equivalent width of the Na I 819 nm absorption band versus de-reddened (V–I) $_0$ colour for field **m11** (**m6**) RGB stars and dwarf stars [bold diamonds (circles) and crosses, respectively]. Bold and thin contours show 10%, 50%, and 90% enclosed fractions for RGB and dwarf stars PDFs, respectively. (**d**) Same as (**c**) for the photometric metallicity estimate (CMD based) versus spectroscopic metallicity estimate (based on the strength of the 850 nm Ca II triplet). The dot-dashed diagonal line shows the one-to-one relation. It is reassuring that the distribution of M31 RGB stars in all four panels follows the RGB PDF and not the dwarf PDF.



Right Ascension: $\alpha[J2000.0]$

